Unraveling the role of protein dynamics in dihydrofolate reductase catalysis

Louis Y. P. Luk[a,1], J. Javier Ruiz-Pernía[b,1], William M. Dawson[a], Maite Roca[b], E. Joel Loveridge[a], David R. Glowacki[c], Jeremy N. Harvey[c], Adrian J. Mulholland[c,2], Iñaki Tuñón[d,2], Vicent Moliner[b,2], and Rudolf K. Allemann[a,2]

[a]School of Chemistry and Cardiff Catalysis Institute, Cardiff University, Cardiff CF10 3AT, United Kingdom; [b]Departament de Química Física i Analítica, Universitat Jaume I, 12071 Castelló, Spain; [c]Centre for Computational Chemistry, School of Chemistry, University of Bristol, Bristol BS8 1TS, United Kingdom; and [d]Departament de Química Física, Universitat de València, 46100 Burjassot, Spain

Edited* by Donald G. Truhlar, University of Minnesota, Minneapolis, MN, and approved August 9, 2013 (received for review July 3, 2013)

Protein dynamics have controversially been proposed to be at the heart of enzyme catalysis, but identification and analysis of dynamical effects in enzyme-catalyzed reactions have proved very challenging. Here, we tackle this question by comparing an enzyme with its heavy (^{15}N, ^{13}C, ^{2}H substituted) counterpart, providing a subtle probe of dynamics. The crucial hydride transfer step of the reaction (the chemical step) occurs more slowly in the heavy enzyme. A combination of experimental results, quantum mechanics/molecular mechanics simulations, and theoretical analyses identify the origins of the observed differences in reactivity. The generally slightly slower reaction in the heavy enzyme reflects differences in environmental coupling to the hydride transfer step. Importantly, the barrier and contribution of quantum tunneling are not affected, indicating no significant role for "promoting motions" in driving tunneling or modulating the barrier. The chemical step is slower in the heavy enzyme because protein motions coupled to the reaction coordinate are slower. The fact that the heavy enzyme is only slightly less active than its light counterpart shows that protein dynamics have a small, but measurable, effect on the chemical reaction rate.

kinetics | computational chemistry | biological chemistry | biophysics | quantum biology

There is heated debate about the role of protein dynamics in enzyme catalysis, especially for reactions that involve transfer of hydrogen (H^+, $H\cdot$, H^-), in which quantum tunneling is significant. It has been suggested that "promoting protein motions", i.e., specific fluctuations that might reduce the barrier height or promote tunneling by reducing donor–acceptor distances, can drive enzymatic reactions (1, 2). Such models include promoting vibrations (3), environmentally coupled tunneling (1), and vibrationally enhanced ground-state tunneling (4). Several of these proposals suggest that the anomalous temperature and pressure dependences of experimentally observed reaction rates and kinetic isotope effects are the consequence of protein motions on the pico- to femtosecond timescale that reduce the width and/or height of the potential energy barrier along the chemical reaction coordinate. However, a connection between promoting motions and potential energy barrier modulation has never been demonstrated directly, and recent work has shown that the temperature dependence of kinetic isotope effects can be accounted for by conformational effects for a number of enzymes (5). Whereas some authors postulate dynamics as a key driving force in catalysis (1–4), others have performed analyses showing activation free-energy reduction, which is an equilibrium property, to be the source of catalysis (6–14). Enzyme reactions, and particularly their dynamics, present formidable challenges for study, and progress requires a combination of theoretical, experimental, and computational approaches (5, 15–18).

Dihydrofolate reductase (DHFR) has been at the heart of the debates about the relationship between enzyme dynamics and catalysis. DHFR catalyses the NAPDH-dependent reduction of 7,8-dihydrofolate (H_2F) to 5,6,7,8-tetrahydrofolate (H_4F) by hydride transfer from C4 of NADPH and protonation of N5 of H_2F. The enzyme from *Escherichia coli* (EcDHFR) cycles through five reaction intermediates, namely E·NADPH, E·NADPH·H_2F, E·$NADP^+$·H_4F, E·H_4F, and E·NADPH·H_4F (19), and adopts two major conformations, the closed conformation in the reactant complexes E·NADPH and E·NADPH·H_2F and the occluded conformation in the three product complexes E·$NADP^+$·H_4F, E·H_4F, and E·NADPH·H_4F (20). The physical steps of ligand association and dissociation have been shown to depend on movements between these two conformations (20, 21). The actual chemical step of hydride transfer from NADPH to H_2F occurs with a reaction-ready configuration of the closed complex (Fig. 1), where the M20 loop (residues 8–23) closes over the active site to shield the reactants from solvent and provide an optimal geometry and electrostatic environment of the active site for the reaction (6, 20). Results for mutants of DHFR (22–25) have been interpreted as showing a central role for protein dynamics in catalysis. However, mutations that affect protein dynamics may actually influence the chemical reaction in other ways (7), such as through changing conformational preferences of the enzyme (26). Strong evidence exists against a direct coupling of large-scale millisecond protein motions to the reaction coordinate during hydride transfer from NADPH to H_2F (6, 7, 27–29), but the coupling of short-range promoting enzyme motions to the reaction coordinate in DHFR cannot be excluded experimentally (6, 22, 27). The effects of protein dynamics on chemical reactions in enzymes have previously been investigated directly only by simulations. These have found that the effects of mutation on reaction in DHFR are not dynamical; rather, the free-energy barrier for reaction is affected (7, 30, 31). Given the lack of clear evidence of dynamical effects on the reaction per se, more direct probes are required.

Significance

The role of protein dynamics in enzyme catalysis remains a topic of considerable debate. Here, we use a combination of experimental and computational methods to identify the origins of the observed changes in reactivity on isotopic substitution of dihydrofolate reductase from *Escherichia coli*. Isotopic substitution causes differences in environmental coupling to the hydride transfer step and protein dynamics have therefore a small but measurable effect on the chemical reaction rate.

Author contributions: E.J.L., A.J.M., I.T., V.M., and R.K.A. designed research; L.Y.P.L., J.J.R.-P., W.M.D., M.R., and D.R.G. performed research; L.Y.P.L., J.J.R.-P., M.R., E.J.L., D.R.G., J.N.H., A.J.M., I.T., V.M., and R.K.A. analyzed data; and E.J.L., D.R.G., J.N.H., A.J.M., I.T., V.M., and R.K.A. wrote the paper.

The authors declare no conflict of interest.

*This Direct Submission article had a prearranged editor.

Freely available online through the PNAS open access option.

[1]L.Y.P.L. and J.J.R.-P. contributed equally to this work.

[2]To whom correspondence may be addressed. E-mail: allemannrk@cf.ac.uk, moliner@uji.es, ignacio.tunon@uv.es, or adrian.mulholland@bris.ac.uk.

This article contains supporting information online at www.pnas.org/lookup/suppl/doi:10.1073/pnas.1312437110/-/DCSupplemental.

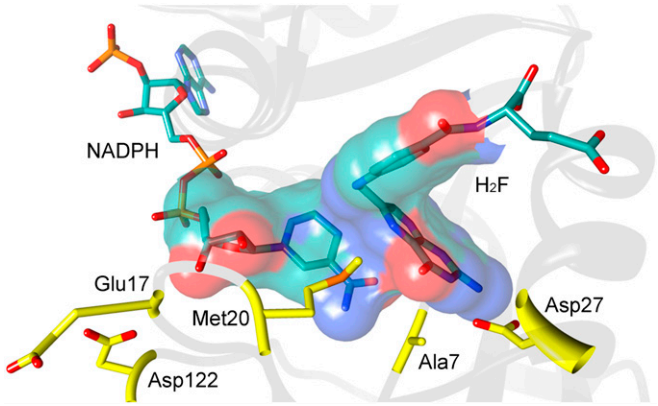

Fig. 1. Active site of EcDHFR in the reaction-ready configuration. Substrate, cofactor, and key amino acid residues are shown as sticks. The portion of the reactants treated quantum mechanically in the QM/MM simulations (*SI Text*) is shown in an overlaid surface representation. The figure was created from the crystal structure with PDB code 1RX2, using UCSF Chimera (60).

Dynamical effects can be rigorously defined as deviations of phenomenological rate constants, $k(T)$, from the predictions of transition-state theory (TST) (32–34). In a canonical ensemble, phenomenological rate coefficients are typically represented as

$$k(T) = \Gamma(T)\frac{k_B T}{h}\cdot\frac{Q^{TS}}{Q^{R}}\exp\left(-\frac{\varepsilon^{TS}}{RT}\right) = \Gamma(T)\frac{k_B T}{h}\cdot\exp\left(-\frac{\Delta G^{QC}_{act}}{RT}\right), \quad [1]$$

where R is the ideal gas constant, k_B is the Boltzmann constant, h is Planck's constant, Q^{TS} and Q^{R} are the respective transition-state (TS) and reactant (R) partition functions, ε^{TS} is the classical transition-state barrier height, ΔG^{QC}_{act} is the quasiclassical activation free energy (for more detail see *SI Text*) (35), and $\Gamma(T)$ is the temperature-dependent transmission coefficient, which generally lumps together the so-called "dynamical" corrections to the classical TST expression. In the limit of classical TST, $\Gamma(T)$ in Eq. **1** is equal to unity. In such circumstances, an Arrhenius plot of $\ln(k(T))$ vs. $1/T$ should be nearly linear, as long as the temperature range is small enough that the preexponential factor is approximately constant.

Several enzymes show nonlinear Arrhenius plots for H-transfer reactions (5, 36–40). However, the microscopic origin of these nonlinearities remains an open question. The most common explanations invoke recrossing and tunneling, both of which are folded into $\Gamma(T)$,

$$\Gamma(T) = \gamma(T)\kappa(T), \quad [2]$$

where the recrossing transmission coefficient, γ, corrects the rate coefficient for trajectories that recross the dividing surface back to the reactant valley, and the tunneling coefficient, κ, accounts for reactive trajectories that do not reach the classical threshold energy. In general, $0 \le \gamma(T) \le 1$, with values less than unity arising from the coupling of the reaction coordinate to other coordinates (discussed in further detail below). $\gamma(T)$ can be estimated from molecular dynamics (MD) trajectories starting from the TS with a thermal distribution of velocities. Recent studies on several enzyme-catalyzed reactions (11–14) suggest that recrossing coefficients tend to be somewhat closer to unity than the corresponding counterpart reactions in solution. In general, $\kappa(T) \ge 1$, with values larger than unity when quantum tunneling is important (41, 42).

Isotopic substitution of substrates or cofactors has provided strong evidence for quantum tunneling in enzyme reactions. The temperature and pressure dependences of experimentally observed reaction rates and kinetic isotope effects have been interpreted to be a consequence of protein motions on the pico- to femtosecond timescale that reduce the width and/or height of the potential energy barrier along the chemical reaction coordinate (1–4, 43). Others have postulated that millisecond conformational fluctuations may also be involved in driving the chemical step of the reaction (22). To focus more directly on protein dynamics, rather than dynamics of the reactants, entire enzymes can be isotopically substituted, with all nonexchangeable atoms of a particular type (e.g., N, C, H) replaced by a heavier isotope; the "heavy" enzyme can then be compared with its natural, lighter counterpart. Within the Born–Oppenheimer approximation, the electronic potential energy surface, V, governing atomic motion is identical in the light and heavy enzymes. The forces acting on the atoms are also identical, being the negative gradient of the potential with respect to atomic coordinates (i.e., $-dV/d\mathbf{q} = F$, where F is the force acting on an atom and $\mathbf{q}$ is a vector of atomic coordinates). Consequently, any differences in reaction rate between the light and heavy enzymes must arise from mass-induced differences in atomic motions, ranging from fast bond vibrations on the femtosecond timescale to conformational changes on the millisecond timescale.

Isotopic substitution of HIV protease, purine nucleoside phosphorylase, alanine racemase, and pentaerythritol tetranitrate reductase has been proposed to affect catalysis by changing ultrafast vibrations that couple to the reaction coordinate (44–47). However, the precise manner in which such mass-dependent effects impact the different terms of the preexponential factor in Eq. **1** remains uncertain. Exactly how $\gamma(T)$ and $\kappa(T)$ contribute to $\Gamma(T)$, and in particular how these are affected by protein dynamics, remains a fundamental and hotly debated question with important consequences for understanding enzyme catalysis. Using a combination of experiment, theory, and computation, we analyze dynamical effects by comparing the rate coefficients for hydride transfer in NADPH catalyzed by both "heavy" (^{15}N, ^{13}C, ^{2}H isotopically substituted) and "light" (natural isotopic abundance) EcDHFR. We have measured, analyzed, and simulated the temperature dependence of the EcDHFR-catalyzed hydride transfer from NADPH to H_2F in the heavy and light enzymes. A key component of these experiments is the fact that we isotopically modified only the protein, leaving the substrate unchanged. This universal isotopic substitution of the protein provides an exquisitely sensitive means of probing dynamical effects.

Results and Discussion

Creation of Heavy EcDHFR. Heavy EcDHFR was produced in M9 medium containing exclusively $^{15}NH_4Cl$, U-^{13}C,^{2}H-glucose, and $^{2}H_2O$. All exchangeable ^{2}H atoms were replaced by ^{1}H during enzyme purification and storage in buffers made of $^{1}H_2O$. The observed 10.76% increase in molecular mass for purified heavy EcDHFR (*SI Text*) showed that 98.6% of the ^{14}N, ^{12}C, and nonexchangeable ^{1}H atoms (76% of total ^{1}H atoms) had been replaced by their heavier isotopes. The circular dichroism spectra of light and heavy EcDHFR were indistinguishable, indicating that the isotope substitution did not alter the overall structure of the protein (Fig. S1).

Experimental Results. The experimentally measured kinetics (Fig. 2 and Tables S1–S3) show intriguing differences in reactivity between the light and heavy enzymes under otherwise identical conditions (*SI Text*). The EcDHFR reaction is strongly dependent on pH; at pH 7, hydride transfer from the reduced cofactor NADPH to (mostly) protonated dihydrofolate is a fast step in the overall turnover of H_2F. At pH values of 9.5 and above, hydride transfer to (mostly) unprotonated substrate is rate limiting (19). At elevated values of pH, the hydride transfer can therefore be monitored in multiple-turnover steady-state

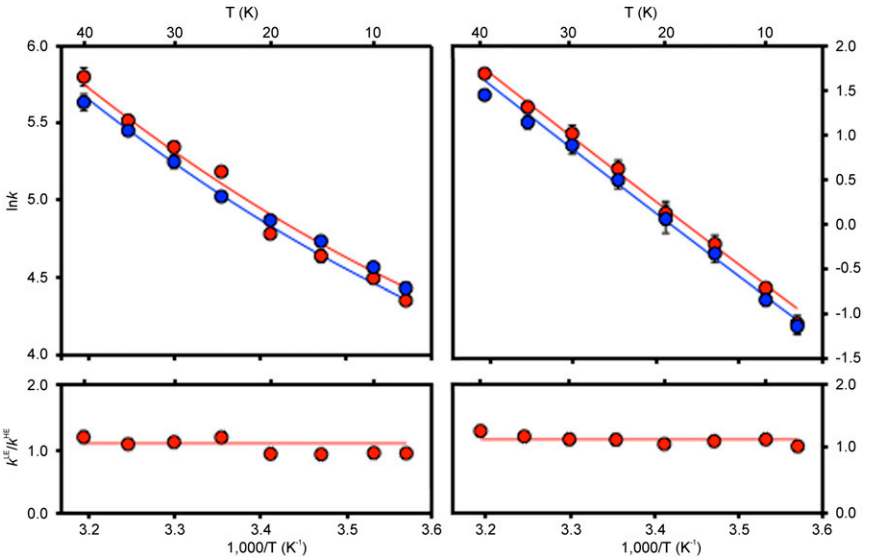

Fig. 2. Experimental EcDHFR data for hydride transfer rate constants and corresponding fits using a tunneling model (5) (V^{TS} = 15 kcal·mol^{-1}) at pH 7 and pH 9.5 (main text). *Upper Left* shows the pH 7.0 pre–steady-state kinetic data (ln k_H^{LE} as red circles and ln k_H^{HE} as blue circles); *Upper Right* shows the pH 9.5 steady-state kinetic data (ln k_{cat}^{LE} as red circles and ln k_{cat}^{HE} as blue circles). Fits to the light and heavy enzyme data are shown using red and blue lines, respectively. *Lower Left* and *Lower Right* show the KIE (ratio of light to heavy enzyme rate constants, k^{LE}/k^{HE}), at pH 7.0 and pH 9.5, respectively, with red circles showing experimental data and the line indicating the fit from the tunneling TST model.

experiments. The steady-state rate constants at pH 9.5 for light and heavy EcDHFR, k_{cat}^{LE} and k_{cat}^{HE}, are similar at low temperatures, but notably diverge with increasing temperature because the rate constants of the light enzyme increase more rapidly (Table S1 and Fig. 2). At 40 °C, k_{cat}^{LE} is 27% larger than k_{cat}^{HE} (Table S1). Michaelis constants for NADPH and dihydrofolate are identical within error for the heavy and light enzymes at both 20 °C and 35 °C (Table S2), suggesting that binding interactions are unaltered in the heavy enzyme. The difference between k_{cat}^{LE} and k_{cat}^{HE} therefore reflects a difference in reactivity between the light and heavy enzymes after formation of the respective Michaelis complexes.

At pH 7.0, the overall turnover rate is determined by release of tetrahydrofolate from the EcDHFR·NADPH·H_4F mixed ternary complex (19). Crystal structures and NMR spectroscopy have revealed that this is accompanied by movement of the M20 and βFG loops with rates similar to those for product release and therefore k_{cat} (20, 21, 48). The enzyme kinetic isotope effects on k_{cat} ($KIE_{cat} = k_{cat}^{LE}/k_{cat}^{HE}$) measured here at pH 7 are in agreement with these observations. Whereas the Michaelis constants were not sensitive to enzyme isotopic substitution, the steady-state rate constants of the light and heavy enzymes (Table S1) showed KIE_{cat} of 1.04 ± 0.03 and 1.16 ± 0.01 at 20 °C and 35 °C, respectively.

To determine the rates of the fast hydride transfer from reduced NADPH to (mostly) protonated dihydrofolate at physiological pH, pre–steady-state stopped-flow experiments that follow the fluorescence resonance energy transfer from the protein to reduced NADPH were conducted. We have shown previously that these are the most physiologically relevant conditions for hydride transfer measurements (29). The rate constants, k_H^{LE} and k_H^{HE}, for hydride transfer catalyzed by the light and heavy enzymes show a similar dependence on temperature to that observed in the steady-state measurements at elevated pH (Table S1 and Fig. 2). The (enzyme) kinetic isotope effect ($KIE_H = k_H^{LE}/k_H^{HE}$) increased from 0.93 ± 0.02 at 10 °C to 1.18 ± 0.06 at 40 °C (Fig. 2). Measurements of the pH dependence of the pre–steady-state rate coefficients for hydride transfer indicated that the apparent pK_a value of the reaction was not affected by isotopic substitutions (Table S3). The apparent pK_a values were 6.26 ± 0.15 and 6.67 ± 0.31 for the light and heavy EcDHFR-catalyzed reactions at 20 °C and 6.40 ± 0.11 and 6.55 ± 0.37 at 35 °C.

Data Fitting. Curvature in the Arrhenius plots (Fig. 2), especially in the pH 7.0 data, hints at microscopic effects beyond those described by simple classical TST. Recently, we have shown that the temperature dependence of rate constants and KIEs in several enzymes can be described using physically reasonable kinetic models that include tunneling corrections (5, 49). For some enzymes, such as aromatic amine dehydrogenase and methylamine dehydrogenase, two conformations with different reactivity are required to reproduce observed behavior, whereas for others like soybean lipoxygenase-1, a single conformation is sufficient. The experimental data in Fig. 2 can be fitted well, using a one-conformation tunneling model of the form

$$k^{HE}(T) = \kappa^{HE}(T) C^{HE} T \exp\left(-\varepsilon^{HE}/RT\right)$$
$$k^{LE}(T) = \kappa^{LE}(T) C^{LE} T \exp\left(-\varepsilon^{LE}/RT\right), \quad [3]$$

where k^{HE} and k^{LE} are the respective temperature-dependent rate constants for hydride transfer in heavy and light EcDHFR, κ^{HE} and κ^{LE} are the tunneling transmission coefficients in the heavy and light enzymes (calculated from an analytical expression for tunneling through a one-dimensional barrier as discussed in *SI Text*), $C^{HE}T$ and $C^{LE}T$ are prefactors that fold in the effect of both recrossing and temperature-dependent contributions of the reaction entropy to the total rate coefficient, and ε^{HE} and ε^{LE} are the enthalpic activation barriers for hydride transfer. The fitting procedure gives excellent agreement with experiment over the entire temperature range (Table S4, Fig. 2, and Fig. S2).

Molecular Dynamics Simulations. Separately, we carried out quantum mechanics/molecular mechanics (QM/MM) molecular dynamics simulations at 300 K with the substrate dihydrofolate fully protonated, to investigate the intricate molecular details of the reaction (Fig. S3). QM/MM ensemble-averaged variational TST (EA-VTST) calculations with multidimensional tunneling corrections have provided useful insight into many enzyme-catalyzed reactions (9, 12, 14, 41, 50). For the molecular dynamics simulations, the reaction coordinate was defined as the difference of distances between the transferred hydride and the

donor and acceptor atoms. Simulations of the heavy enzyme were performed using the masses of ^{15}N, ^{13}C, and ^{2}H for nitrogen, carbon, and nonexchangeable hydrogen atoms. Structures from the QM/MM molecular dynamics simulations were used for EA-VTST calculations, which work out $\Gamma(T)$ by calculating both γ and κ (Eqs. **1** and **2**) (further details in *SI Text*).

The extent of dynamical coupling between the reaction coordinate and other motions within the protein–substrate complex is indicated by the magnitude of the recrossing coefficient, γ. It is important to point out that the calculated value of γ is related to the free-energy profile (51). The free-energy profile in turn depends on the choice of the reaction coordinate. Here, we confine our discussion to the difference in the distances between the transferred hydride and its donor/acceptor. The reasons for this are twofold: (*i*) The extent to which our recrossing coefficients deviate from unity is comparable to that in previous studies (11, 12, 30), suggesting that we have chosen a reasonable reaction coordinate, and (*ii*) a reaction coordinate based on bond distances conforms to the local mode picture that chemists typically use to rationalize whether or not a reaction has occurred. In *SI Text*, we describe more sophisticated quantized variational transition state searches carried out on the mass weighted coordinates of larger atomic subsets surrounding the hydride transfer region. The important point of these additional tests is that the free-energy profiles for hydride transfer in both the light and the heavy systems are statistically identical for the reaction coordinates that we investigated. As shown in *SI Text* (e.g., Fig. S4*B*), changes in the reaction coordinate significantly affect neither the height nor the position of the free-energy maximum, in agreement with the results of the experimental fits described above.

Discussion

The 300-K classical potentials of mean force (PMF), obtained using the semiempirical Austin Model 1 Hamiltonian with specific reaction parameters and molecular mechanics (AM1-SRP/MM), give free-energy barriers that are statistically identical in the heavy and light enzymes and close to the value of 15 kcal·mol^{-1} obtained above for the classical barrier height (V^{TS}) through fits to the experimental data (*SI Text*). This value is considerably different from the activation energy of ~6.3 kcal·mol^{-1} obtained using an Arrhenius-type fit (Table S4), providing an excellent cautionary example of how Arrhenius-type fits can be misleading when $\Gamma(T)$ is significant. The quantized vibrational corrections to the reactant PMF are small and statistically indistinguishable in the heavy and light enzymes (*SI Text*). The findings from the QM/MM MD simulations are consistent with the kinetic fits, which found ε^{LE} and ε^{HE} to be very similar at each pH and within 1.2 kcal·mol^{-1} of V^{TS} (Table S4). The magnitude of these corrections is similar to those found in previous studies on hydride transfer reactions in other NAD(P)H-dependent enzymes (52–54). The 300-K rate constants obtained from MD simulations, which result directly from the simulations without any fitting to the experimental data, are in excellent agreement with the experimental values (which are of course themselves subject to some uncertainty) (Table 1). It is important to note that such good agreement (apparently within the errors of all of the various methods) is, to some extent, fortuitous given the complexity of simulating enzyme reactions. Nevertheless, these results (taken alongside the kinetic modeling) suggest that the computational approach is reasonable.

The EA-VTST tunneling coefficients, κ, are statistically identical for the heavy and light enzymes (Table 1), with an effective contribution to the phenomenological barrier less than 1 kcal·mol^{-1}. Qualitatively, this result is identical to that found from fitting the kinetic data: The best-fit values for ω^{LE} and ω^{HE} (Table S4) suggest a barrier that is rather broad and smooth. The tunneling coefficients obtained from EA-VTST and independently from the fitting model agree within errors (Table S4), both methods suggesting that contributions from tunneling in the heavy and light enzymes are small and effectively identical. The EA-VTST values of the barrier reduction due to tunneling are also very close to those calculated for DHFR from *Thermotoga maritima* (*ca*. 0.7 kcal·mol^{-1}, computed for the monomer at 298 K) (16) and for lactate dehydrogenase (*ca*. 0.8 kcal·mol^{-1}) (55), but slightly smaller than those found for thymidylate synthase (1.4 kcal·mol^{-1} for hydride transfer at 303 K) (14) or morphinone reductase (1.5 kcal·mol^{-1} for hydride transfer at 298 K) (56). In both light and heavy enzymes, the time-dependent flux–flux correlation functions used to obtain the transmission coefficients show a fast decay during the first 20 fs and a subsequent plateau after 40–60 fs (Fig. S4*C*), giving 0.57 for γ^{LE} and 0.49 for γ^{HE}. This corresponds to a γ^{LE}:γ^{HE} ratio of 1.16, in good agreement with the results of the fitting, in which the preexponential factors C^{LE} and C^{HE} have a ratio of 1.14 at pH 9.5 and 1.08 at pH 7.

The fits and the QM/MM results both point to a scenario in which the difference in phenomenological rate constants between the heavy and light enzymes arises in part from the different participation of protein motions in the reaction coordinate. In the EA-VTST model, this is captured through differences in the recrossing coefficients γ, whereas in the fitting model differences in γ are folded into differences in C^{LE} and C^{HE}. The origin of the difference in the recrossing coefficients lies in the coupling between the reaction coordinate and the environmental motions. In general, the coupling of environmental modes to motion along the reaction coordinate depends on the relative values of each mode's frequencies. The speed of passage over the TS is largely determined by the curvature of the energy surface around the TS. In general, environmental motions characterized by vibrational frequencies that are greater than or equal to the equivalent characteristic time for passage through the transition state region quickly adapt to geometrical changes in the reaction coordinate, and the fast equilibrium assumption (implicit in TST) holds. Environmental motions characterized by vibrational frequencies less than the characteristic time for passage over the reaction coordinate reaction frequency adapt to geometrical changes along the reaction coordinate more slowly and the fast equilibrium assumption becomes less valid. In ergodic systems, faster environmental response is therefore often linked to higher-energy frequency distributions. The friction spectrum (Fig. S4*D*) shows the distribution of frequencies that couple to the reaction coordinate in both the heavy and the light enzymes. Qualitatively, the most significant differences between the friction spectra in both systems occur below frequencies of ~1,000 cm^{-1} (with many

Table 1. Transmission coefficient components due to recrossing (γ) and tunneling (κ) for hydride transfer in light and heavy EcDHFR, determined by QM/MM calculations

EcDHFR	γ	κ	ΔG^{QC}_{act}, kcal·mol^{-1}	ΔG_{eff}, kcal·mol^{-1}	k_{theor}, s^{-1}	k_{exp}, s^{-1}
Light	0.57 ± 0.02	2.61 ± 0.49	14.59 ± 0.41	14.35 ± 0.54	219	209.1 ± 5.0
Heavy	0.49 ± 0.02			14.46 ± 0.54	188	190.1 ± 8.5

ΔG^{QC}_{act} is the quasiclassical (QC) free energy of activation (Eq. **1**); ΔG_{eff} is the effective phenomenological free energy of activation, into which the effects of tunneling and recrossing are folded; k_{theor} is the predicted hydrogen transfer rate coefficient at 300 K; and k_{exp} is the experimentally determined hydrogen transfer rate coefficient at 303 K.

of the most intense peaks in the heavy enzymes red-shifted by ~30 cm^{-1} compared with the light enzyme, owing to the greater masses). The lower frequency distribution in the heavy enzyme system is consistent with a slower environmental response time in the heavy protein and a transmission coefficient that has a correspondingly larger departure from unity.

The MD simulations suggest that differences in the environmental response time between the heavy and light proteins translate to an effective free-energy difference in the barrier heights for hydride transfer, with the barrier in the light enzyme 0.11 kcal·mol^{-1} lower than that in the heavy enzyme at 300 K (Table 1). Within the error limits at 300 K, the recrossing factor γ captures most of the difference between the experimentally observed $k(T)$ values in the heavy and light enzymes.

To investigate possible dynamical differences between the light and heavy enzymes, we examined isolated dynamical observables either side of the transition state calculated from the QM/MM simulations of hydride transfer in each enzyme (Table S5). These reveal that the light and heavy enzymes are very similar, with little or no significant difference in many dynamical observables. For example, the donor–acceptor distance (Fig. S4*E*) and the angle between the donor, hydride, and acceptor atoms (Fig. S4*F*) in the heavy and light systems show very similar time-dependent profiles. Other distances between atoms in the substrate and the active site during reaction also show similar behavior in the heavy and light enzymes: The approach of Met20 to the substrate and the amide group of the cofactor nicotinamide ring (Fig. S4*G*), which precedes the formation of the TS [and has been suggested to stabilize the hydride transfer TS (57)], has very similar time profiles in the light and heavy enzymes. Compelling evidence for a faster environmental response in the light enzyme is clearly seen only with a global analysis that accounts for all atomic positions within both the light and the heavy enzyme. The root mean squared deviation (RMSD) along reactive trajectories between the average geometry at time t and the average TS geometry (Fig. S4*H*) shows that the global environmental response is slightly faster in the light enzyme, as deduced from the exponential decays of the RMSD on both enzymes. The relaxation rate constants obtained from a least-squares fit are 9.0 ± 0.1 ps^{-1} and 8.7 ± 0.1 ps^{-1} for the light and heavy enzymes, respectively.

Most significantly, analysis of the RMSD reveals that the light enzyme environment—taken as a global aggregate—responds more quickly to motion along the reaction coordinate (Fig. S4*H*). It is also interesting to consider the converse: namely, how the reaction coordinate responds to motions in the environment. Thermodynamic detailed balance requires that a faster response in one direction must be linked to a faster response in the reverse direction—i.e., the chemical reaction rate in the light enzyme must be more responsive to environmental fluctuations and perturbations than that in the heavy enzyme. For DHFR, protein motion couples to the reaction coordinate in a rather subtle way that is apparent only via a global description of all atomic positions. This makes it difficult to specifically identify any "promoting motions" that couple EcDHFR motions to progress along the reaction coordinate. Clearly any dynamical effects on the chemical step are small, subtle, and not localized, but apparently play a role in making the heavy enzyme less active than its natural, light counterpart. Unraveling the microscopic mechanisms responsible for this sort of global dynamical coupling offers interesting and fertile territory for future investigations into the microscopic mechanisms that underlie enzyme function. Work is currently underway to investigate the effect of isotopically labeling segments of EcDHFR to determine whether certain portions of the enzyme play a greater role in the dynamical effects.

Conclusions

Our experimental results show that hydride transfer from NADPH to dihydrofolate is generally somewhat faster in light EcDHFR than in its heavy counterpart, over the temperature range 280–313 K. Fitting this temperature-dependence data to a recently developed model based on TST suggests that both the tunneling contributions and the barrier heights in the heavy and light enzymes are identical; the fitting indicates that the differences in the rate coefficients arise from variations in the respective preexponential factors. This conclusion is supported by QM/MM MD simulations and EA-VTST calculations carried out at 300 K, which suggest that (*i*) the tunneling probabilities and barrier heights are statistically indistinguishable in the light and heavy enzymes and (*ii*) the differences in the phenomenological rate coefficients are mostly accounted for by differences in the recrossing coefficient. Thus, the difference in reactivity is due neither to differences in quantum tunneling nor to differences in barrier height, but rather to differences in the extent to which the protein environment of the light and heavy enzymes globally couples to the reaction coordinate. These findings run counter to proposals that invoke enhancement of tunneling or barrier modulation by specific protein ("promoting") motions or claims that protein dynamics "drive" tunneling.

Although TST with tunneling corrections broadly accounts for the observed hydride transfer rate coefficients, more detailed quantitative analysis requires dynamical recrossing corrections. Specifically, our simulations and modeling indicate that the main cause of the difference in the rate constants for the reactions catalyzed by light and heavy EcDHFR is different coupling of global motions with the protein environment along the reaction coordinate. In a TST treatment this can be translated into a slightly different reaction coordinate (e.g., a more global coordinate allowing more of the protein to participate directly) or, more conveniently in this case, into a different value of the recrossing transmission coefficient. Irrespective of this procedural choice, our experimental and theoretical results agree that the small differences in reactivity between the light and heavy enzymes most probably arise from differences in the extent to which the protein environment is coupled to the chemical step. In the light enzyme, where atomic motion is characterized by higher frequencies, the environment responds more rapidly to changes along the reaction coordinate, resulting in fewer trajectory recrossings. This study, which compares kinetics in the light and heavy enzymes, provides important insight into the nature of enzyme reaction dynamics. Although protein dynamics have a measurable effect on the chemical reaction, the effect is relatively small and is not related to differences in quantum tunneling.

Methods

Experimental Methods. EcDHFR and ^{15}N-, ^{13}C-, ^{2}H-labeled (heavy) EcDHFR were produced in M9 medium and purified as previously described (58). Electrospray ionization mass spectrometry was used to determine the degree of isotopic substitution in the heavy enzyme, and structural integrity was confirmed by circular dichroism spectroscopy. Steady-state and stopped-flow kinetic measurements were performed as previously described (38, 59).

Fitting Methodology. The temperature-dependent experimental hydride transfer data at different values of pH were fitted to Eq. **3**, using a nonlinear least-squares minimization algorithm. Fitting the data to a more sophisticated multiconformation model did not give improved nonlinear least-squares fits compared with single-conformer models.

QM/MM EA-VTST Calculations and Molecular Dynamics Simulations. Protein Data Bank entry 3QL3 (22) was used as the starting structure for simulations. Heavy EcDHFR was prepared by modifying the masses of all ^{14}N, ^{12}C, and nonexchangeable ^{1}H atoms to those of ^{15}N, ^{13}C, and ^{2}H. QM/MM EA-VTST calculations and molecular dynamics simulations were performed to determine reactive trajectories and to extract contributions to the transmission coefficient (Eq. **2**) and activation parameters.

A full description of experimental, fitting, and simulation methods is provided in *SI Text*.

ACKNOWLEDGMENTS. We acknowledge the computational facilities of Universitat Jaume I and Universitat de València (Tirant Supercomputer).

This work was supported by Grants BB/E008380/1 and BB/J005266/1 (to R.K.A.) from the UK Biotechnology and Biological Sciences Research Council, by Doctoral Training Account funding from the UK Engineering and Physical Sciences Research Council (EPSRC), by the Vice Chancellor Fund of Cardiff University, by the Spanish Ministerio de Economía y Competitividad (Project CTQ2012-36253-C03), by Generalitat Valenciana (Projects ACOMP/2012/119, GV/2012/044, GV/2012/053, and Prometeo/2009/053), and by Universitat Jaume I-Bancaixa (Projects P1·1A2010-08 and P1·1B2011-23). J.J.R.-P. thanks the Spanish Ministerio de Ciencia e Innovación for a "Juan de la Cierva" contract. A.J.M. is an EPSRC Leadership Fellow (Grant EP/G007705/1). D.R.G. has support under EPSRC Programme Grant EP/G00224X/1.

1. Nagel ZD, Klinman JP (2009) A 21st century revisionist's view at a turning point in enzymology. *Nat Chem Biol* 5(8):543–550.
2. Limbach H-H, Schowen KB, Schowen RL (2010) Heavy atom motions and tunneling in hydrogen transfer reactions: The importance of the pre-tunneling state. *J Phys Org Chem* 23:586–605.
3. Antoniou D, Caratzoulas S, Kalyanaraman C, Mincer JS, Schwartz SD (2002) Barrier passage and protein dynamics in enzymatically catalyzed reactions. *Eur J Biochem* 269(13):3103–3112.
4. Scrutton NS, Basran J, Sutcliffe MJ (1999) New insights into enzyme catalysis. Ground state tunnelling driven by protein dynamics. *Eur J Biochem* 264(3):666–671.
5. Glowacki DR, Harvey JN, Mulholland AJ (2012) Taking Ockham's razor to enzyme dynamics and catalysis. *Nat Chem* 4(3):169–176.
6. Loveridge EJ, Behiry EM, Guo J, Allemann RK (2012) Evidence that a 'dynamic knockout' in Escherichia coli dihydrofolate reductase does not affect the chemical step of catalysis. *Nat Chem* 4(4):292–297.
7. Adamczyk AJ, Cao J, Kamerlin SCL, Warshel A (2011) Catalysis by dihydrofolate reductase and other enzymes arises from electrostatic preorganization, not conformational motions. *Proc Natl Acad Sci USA* 108(34):14115–14120.
8. Olsson MHM, Parson WW, Warshel A (2006) Dynamical contributions to enzyme catalysis: Critical tests of a popular hypothesis. *Chem Rev* 106(5):1737–1756.
9. Garcia-Viloca M, Gao J, Karplus M, Truhlar DG (2004) How enzymes work: Analysis by modern rate theory and computer simulations. *Science* 303(5655):186–195.
10. Gao J, et al. (2006) Mechanisms and free energies of enzymatic reactions. *Chem Rev* 106(8):3188–3209.
11. Roca M, Moliner V, Tuñón I, Hynes JT (2006) Coupling between protein and reaction dynamics in enzymatic processes: Application of Grote-Hynes Theory to catechol O-methyltransferase. *J Am Chem Soc* 128(18):6186–6193.
12. Ruiz-Pernía JJ, Tuñón I, Moliner V, Hynes JT, Roca M (2008) Dynamic effects on reaction rates in a Michael addition catalyzed by chalcone isomerase. Beyond the frozen environment approach. *J Am Chem Soc* 130(23):7477–7488.
13. Roca M, Oliva M, Castillo R, Moliner V, Tuñón I (2010) Do dynamic effects play a significant role in enzymatic catalysis? A theoretical analysis of formate dehydrogenase. *Chemistry* 16(37):11399–11411.
14. Kanaan N, et al. (2011) Temperature dependence of the kinetic isotope effects in thymidylate synthase. A theoretical study. *J Am Chem Soc* 133(17):6692–6702.
15. Roston D, Cheatum CM, Kohen A (2012) Hydrogen donor-acceptor fluctuations from kinetic isotope effects: A phenomenological model. *Biochemistry* 51(34):6860–6870.
16. Pang JY, Pu JZ, Gao JL, Truhlar DG, Allemann RK (2006) Hydride transfer reaction catalyzed by hyperthermophilic dihydrofolate reductase is dominated by quantum mechanical tunneling and is promoted by both inter- and intramonomeric correlated motions. *J Am Chem Soc* 128(24):8015–8023.
17. Pu J, Ma S, Gao J, Truhlar DG (2005) Small temperature dependence of the kinetic isotope effect for the hydride transfer reaction catalyzed by Escherichia coli dihydrofolate reductase. *J Phys Chem B* 109(18):8551–8556.
18. Kamerlin SCL, Warshel A (2010) At the dawn of the 21st century: Is dynamics the missing link for understanding enzyme catalysis? *Proteins* 78(6):1339–1375.
19. Fierke CA, Johnson KA, Benkovic SJ (1987) Construction and evaluation of the kinetic scheme associated with dihydrofolate reductase from Escherichia coli. *Biochemistry* 26(13):4085–4092.
20. Sawaya MR, Kraut J (1997) Loop and subdomain movements in the mechanism of Escherichia coli dihydrofolate reductase: Crystallographic evidence. *Biochemistry* 36(3):586–603.
21. Boehr DD, McElheny D, Dyson HJ, Wright PE (2006) The dynamic energy landscape of dihydrofolate reductase catalysis. *Science* 313(5793):1638–1642.
22. Bhabha G, et al. (2011) A dynamic knockout reveals that conformational fluctuations influence the chemical step of enzyme catalysis. *Science* 332(6026):234–238.
23. Wang L, Tharp S, Selzer T, Benkovic SJ, Kohen A (2006) Effects of a distal mutation on active site chemistry. *Biochemistry* 45(5):1383–1392.
24. Agarwal PK, Billeter SR, Rajagopalan PTR, Benkovic SJ, Hammes-Schiffer S (2002) Network of coupled promoting motions in enzyme catalysis. *Proc Natl Acad Sci USA* 99(5):2794–2799.
25. Cameron CE, Benkovic SJ (1997) Evidence for a functional role of the dynamics of glycine-121 of Escherichia coli dihydrofolate reductase obtained from kinetic analysis of a site-directed mutant. *Biochemistry* 36(50):15792–15800.
26. Swanwick RS, Shrimpton PJ, Allemann RK (2004) Pivotal role of Gly 121 in dihydrofolate reductase from Escherichia coli: The altered structure of a mutant enzyme may form the basis of its diminished catalytic performance. *Biochemistry* 43(14):4119–4127.
27. Loveridge EJ, et al. (2011) The role of large-scale motions in catalysis by dihydrofolate reductase. *J Am Chem Soc* 133(50):20561–20570.
28. Loveridge EJ, Tey LH, Allemann RK (2010) Solvent effects on catalysis by Escherichia coli dihydrofolate reductase. *J Am Chem Soc* 132(3):1137–1143.
29. Loveridge EJ, Allemann RK (2011) Effect of pH on hydride transfer by Escherichia coli dihydrofolate reductase. *ChemBioChem* 12(8):1258–1262.
30. Boekelheide N, Salomón-Ferrer R, Miller TF, 3rd (2011) Dynamics and dissipation in enzyme catalysis. *Proc Natl Acad Sci USA* 108(39):16159–16163.
31. Fan Y, Cembran A, Ma S, Gao J (2013) Connecting protein conformational dynamics with catalytic function as illustrated in dihydrofolate reductase. *Biochemistry* 52:2036–2049.
32. Glasstone S, Laidler KJ, Eyring H (1941) *The Theory of Rate Processes: The Kinetics of Chemical Reactions, Viscosity, Diffusion and Electrochemical Phenomena* (McGraw-Hill, New York).
33. Keck JC (1967) Variational theory of reaction rates. *Adv Chem Phys* 13:85–121.
34. Truhlar DG, Garrett BC, Klippenstein SJ (1996) Current status of transition-state theory. *J Phys Chem* 100:12771–12800.
35. Alhambra C, et al. (2001) Canonical variational theory for enzyme kinetics with the protein mean force and multidimensional quantum mechanical tunneling dynamics. Theory and application to liver alcohol dehydrogenase. *J Phys Chem B* 105:11326–11340.
36. Kohen A, Cannio R, Bartolucci S, Klinman JP (1999) Enzyme dynamics and hydrogen tunnelling in a thermophilic alcohol dehydrogenase. *Nature* 399(6735):496–499.
37. Truhlar DG, Kohen A (2001) Convex Arrhenius plots and their interpretation. *Proc Natl Acad Sci USA* 98(3):848–851.
38. Maglia G, Allemann RK (2003) Evidence for environmentally coupled hydrogen tunneling during dihydrofolate reductase catalysis. *J Am Chem Soc* 125(44):13372–13373.
39. Anandarajah K, Schowen KB, Schowen RL (2008) Hydrogen tunneling in glucose oxidation by the archaeon Thermoplasma acidophilum. *Z Phys Chem* 222:1333–1347.
40. Tsai SC, Klinman JP (2001) Probes of hydrogen tunneling with horse liver alcohol dehydrogenase at subzero temperatures. *Biochemistry* 40(7):2303–2311.
41. Masgrau L, et al. (2006) Atomic description of an enzyme reaction dominated by proton tunneling. *Science* 312(5771):237–241.
42. Knapp MJ, Rickert K, Klinman JP (2002) Temperature-dependent isotope effects in soybean lipoxygenase-1: Correlating hydrogen tunneling with protein dynamics. *J Am Chem Soc* 124(15):3865–3874.
43. Major DT, et al. (2009) Differential quantum tunneling contributions in nitroalkane oxidase catalyzed and the uncatalyzed proton transfer reaction. *Proc Natl Acad Sci USA* 106(49):20734–20739.
44. Kipp DR, Silva RG, Schramm VL (2011) Mass-dependent bond vibrational dynamics influence catalysis by HIV-1 protease. *J Am Chem Soc* 133(48):19358–19361.
45. Silva RG, Murkin AS, Schramm VL (2011) Femtosecond dynamics coupled to chemical barrier crossing in a Born-Oppenheimer enzyme. *Proc Natl Acad Sci USA* 108(46):18661–18665.
46. Pudney CR, et al. (2013) Fast protein motions are coupled to enzyme H-transfer reactions. *J Am Chem Soc* 135(7):2512–2517.
47. Toney MD, Castro JN, Addington TA (2013) Heavy-enzyme kinetic isotope effects on proton transfer in alanine racemase. *J Am Chem Soc* 135(7):2509–2511.
48. Falzone CJ, Wright PE, Benkovic SJ (1994) Dynamics of a flexible loop in dihydrofolate reductase from Escherichia coli and its implication for catalysis. *Biochemistry* 33(2):439–442.
49. Glowacki DR, Harvey JN, Mulholland AJ (2012) Protein dynamics and enzyme catalysis: The ghost in the machine? *Biochem Soc Trans* 40(3):515–521.
50. Pu J, Gao J, Truhlar DG (2006) Multidimensional tunneling, recrossing, and the transmission coefficient for enzymatic reactions. *Chem Rev* 106(8):3140–3169.
51. Truhlar DG, et al. (2004) Ensemble-averaged variational transition state theory with optimized multidimensional tunneling for enzyme kinetics and other condensed-phase reactions. *Int J Quantum Chem* 100:1136–1152.
52. Garcia-Viloca M, Alhambra C, Truhlar DG, Gao J (2001) Inclusion of quantum-mechanical vibrational energy in reactive potentials of mean force. *J Chem Phys* 114:9953–9958.
53. Alhambra C, Corchado JC, Sanchez ML, Gao JL, Truhlar DG (2000) Quantum dynamics of hydride transfer in enzyme catalysis. *J Am Chem Soc* 122:8197–8203.
54. Webb SP, Agarwal PK, Hammes-Schiffer S (2000) Combining electronic structure methods with the calculation of hydrogen vibrational wavefunctions: Application to hydride transfer in liver alcohol dehydrogenase. *J Phys Chem B* 104:8884–8894.
55. Ferrer S, et al. (2006) A theoretical analysis of rate constants and kinetic isotope effects corresponding to different reactant valleys in lactate dehydrogenase. *J Am Chem Soc* 128(51):16851–16863.
56. Pang J, Hay S, Scrutton NS, Sutcliffe MJ (2008) Deep tunneling dominates the biologically important hydride transfer reaction from NADH to FMN in morphinone reductase. *J Am Chem Soc* 130(22):7092–7097.
57. Garcia-Viloca M, Truhlar DG, Gao J (2003) Reaction-path energetics and kinetics of the hydride transfer reaction catalyzed by dihydrofolate reductase. *Biochemistry* 42(46):13558–13575.
58. Hay S, et al. (2009) Are the catalytic properties of enzymes from piezophilic organisms pressure adapted? *ChemBioChem* 10(14):2348–2353.
59. Evans RM, et al. (2010) Catalysis by dihydrofolate reductase from the psychropiezophile Moritella profunda. *ChemBioChem* 11(14):2010–2017.
60. Pettersen EF, et al. (2004) UCSF Chimera—a visualization system for exploratory research and analysis. *J Comput Chem* 25(13):1605–1612.

Supporting Information

Luk et al. 10.1073/pnas.1312437110

SI Text

SI Methods

Chemicals. ^{15}N-ammonium chloride, [$^{13}C_6$,$^{2}H_7$]-glucose, 99.9 atom% $^{2}H_2O$, and folate were purchased from Sigma. NADPH, $NADP^+$, and isopropyl-β-D-thiogalactopyranoside (IPTG) were purchased from Melford. H_2F was prepared by dithionite reduction of folate (1). The concentrations of NADPH and H_2F were determined spectrophotometrically, using extinction coefficients of 6,200 $M^{-1}\cdot cm^{-1}$ at 339 nm and 28,000 $M^{-1}\cdot cm^{-1}$ at 282 nm, respectively (2).

Enzyme Preparation. *Escherichia coli* dyhydrofolate reductase (EcDHFR) and ^{15}N-, ^{13}C-, ^{2}H-labeled (heavy) EcDHFR in M9 medium were prepared using a modification of the protocol described by Falzone et al. (3). *E. coli* BL21(DE3) cells harboring a cDNA for EcDHFR (4) from an overnight culture in LB medium containing 100 μg/mL ampicillin were washed three times with M9 medium and then grown in 1 L M9 medium until the OD_{600} reached 0.6. IPTG (to 0.5 mM) was added and the culture grown to an OD_{600} of 2.0. The cells were harvested and the enzyme was purified as previously described (5). Heavy EcDHFR was produced as described for the unlabeled enzyme in M9 medium in [$^{2}H_2$, 99.9 atom%] H_2O supplemented with 1 g/L [^{15}N, 98 atom%] NH_4Cl and 2 g/L [$^{13}C_6$, 99 atom%; 1,2,3,4,5,6,6-$^{2}H_7$, 97 atom%] glucose. In both cases, "normal" water (i.e., $^{1}H_2O$) was used for purification, so all exchangeable deuterons were replaced by protons. The purity of the enzyme was assessed by SDS/PAGE. Typically ~30 mg of apparently homogenous EcDHFR was obtained from 1 L culture. Enzymes were stored at 4 °C for up to 3 wk without detectable loss of activity. Electrospray ionization mass spectrometry indicated masses of 17,996.5 and 19,933.6 Daltons for light and heavy enzymes, respectively.

Circular Dichroism Spectroscopy. Circular dichroism experiments were performed on an Applied PhotoPhysics Chirascan spectrometer, using 14 μM protein in deoxygenated 10 mM potassium phosphate buffer (pH 7). Spectra (Fig. S1) were measured between 200 nm and 400 nm in 10-mm quartz cuvettes under N_2 with 50 nm/min scan speed, 0.5 nm data pitch, 1 nm bandwidth, and 0.5 s response time.

Steady-State Kinetic Measurements. Steady-state kinetic measurements (Table S1) were performed on a JASCO V-660 spectrophotometer as described in ref. 6, monitoring the decrease in absorbance at 340 nm during the reaction [ε_{340} (NADPH + H_2F) = 11,800 $M^{-1}\cdot cm^{-1}$] (7). The steady-state turnover rates of EcDHFR were determined at pH 7 and pH 9.5 in MTEN buffer (50 mM morpholinoethanesulfonic acid, 25 mM Tris, 25 mM ethanolamine, 100 mM NaCl, and 10 mM β-mercaptoethanol), using 30 nM enzyme. The pH was carefully adjusted at each experimental temperature to account for the temperature dependence of the pK_a of organic amines. The enzyme was preincubated with NADPH (100 μM) at the desired temperature for 5 min before addition of H_2F (100 μM). Each data point is the result of three independent measurements. To determine Michaelis constants (Table S2), concentrations of NADPH were varied between 3 μM and 100 μM (pH 7) or between 1 μM and 100 μM (pH 9.5), and concentrations of H_2F were varied between 0.5 μM and 100 μM, while keeping the concentration of the other reactant fixed at 100 μM.

Pre–Steady-State Kinetic Measurements. Hydride transfer rate constants (Tables S1 and S3) were measured under single-turnover conditions on a Hi-Tech Scientific stopped-flow spectrophotometer essentially as described before (8). Before mixing, the enzyme (40 μM) was preincubated with NADPH (16 μM) for at least 1 min in 100 mM potassium phosphate containing 100 mM NaCl and 10 mM β-mercaptoethanol at pH 7 or in MTEN buffer for pH-dependent measurements, and the reaction started by rapidly mixing with H_2F (200 μM) in the same buffer. Where MTEN buffer was used, the pH was carefully adjusted at each experimental temperature to account for the temperature dependence of the pK_a of organic amines. Reduction of the fluorescence resonance energy transfer from the enzyme to NADPH during the reaction was measured by exciting the sample at 297 nm and measuring emission using a 400-nm cutoff filter. All measurements were repeated at least six times. Rate constants were extracted by fitting the kinetic data to the equation for a double-exponential decay.

Tunneling Model Fitting Methodology

Using Eq. **3** in the main text, we fitted the temperature-dependent experimental hydride transfer data at different values of pH (pH 7 fits used the pre–steady-state data, and pH 9.5 fits used the steady-state data). $\kappa^{HE}(T)$ and $\kappa^{LE}(T)$ were calculated using an analytic approximation to average energy-dependent Wentzel–Kramers–Brillouin (WKB) transmission coefficients over a thermal Maxwell–Boltzmann distribution (assuming a parabolic barrier shape) (9),

$$\kappa^{\ell}(T) = \frac{\beta}{\beta - \alpha^{\ell}}\left[\exp\left[\left(\beta - \alpha^{\ell}\right)V^{TS}\right] - 1\right], \qquad \textbf{[S1]}$$

where ℓ is an index that denotes the heavy or light enzyme (HE or LE). V^{TS} is the classical transition-state energy, which is uncorrected for zero point energy and thus identical for both isotopomers within the Born–Oppenheimer approximation. $\alpha^{\ell} = 2\pi/(\hbar\omega^{\ell})$, where ω^{ℓ} is the angular velocity corresponding to the transition state frequency (i.e., $\omega = 2\pi\nu$, where ν is the magnitude of the transition-state imaginary frequency), and $\beta = (kT)^{-1}$.

Fitting to the data obtained at each pH was carried out using a nonlinear least-squares minimization algorithm where the total value of χ^2 was calculated using the light enzyme hydride transfer rate constants, $k^{LE}(T)$; the heavy enzyme hydride transfer rate constants, $k^{HE}(T)$; and the corresponding (enzyme) kinetic isotope effects (KIEs), $k^{LE}(T)/k^{HE}(T)$. Each of these datasets is depicted in Fig. 2 of the main text. To reduce the fitting parameter space, we followed similar procedures to those in our previous work (10, 11) and rationally constrained the parameters in Eq. **3** and Eq. **S1** as follows:

i) For light isotope systems, the transition state imaginary frequency generally has a larger magnitude than it does in heavy systems, indicating more significant curvature on the potential energy surface in mass-weighted coordinates. Thus, we specified that $\omega^{LE} \geq \omega^{HE}$, with 1,000 $cm^{-1} < \omega^{LE} < 4{,}000$ cm^{-1}. This range of values is typical of hydride transfer systems (11–14).

ii) Light isotope systems often have a smaller effective ε (enthalpic activation barrier) owing to larger zero-point energies in the reactant vibrations that take the system across the barrier and into the products. Hence we specified that $\varepsilon^{HE} \geq \varepsilon^{LE}$, with both within 10% of V^{TS}.

iii) C^{LE} and C^{HE}, which include the partition function ratio of the transition state to the reactant as well as the recrossing coefficient, differ by no more than an order of magnitude. The typical ratio of vibrational partition functions for isotopically and nonisotopically substituted harmonic oscillators is usually close to unity, far smaller than our constraint.

Even with these constraints, it was initially difficult to converge the fits owing to strong parameter codependencies, as discussed previously (11). The classical barrier height, V^{TS}, is among the most important parameters to derive from the fitting; however, a range of different parameter sets gave reasonably good fits with different values of V^{TS}. In light of this fact, we calculated values of χ^2 by scanning over fixed values of V^{TS}, with all other parameters floated. The fitting method indicates that our fits using Eq. **3** and Eq. **S1** for both pH 7 and pH 9.5 data give χ^2 minima when V^{TS} values are around 15 kcal·mol^{-1} (Fig. S2), in good agreement with the barrier from the classical potential of mean force (PMF) obtained independently from the quantum mechanics/molecular mechanics (QM/MM) molecular dynamics (MD) simulations. Using this optimal V^{TS} value, the best-fit parameters are shown in Table S4, and the corresponding fits produced by these parameters are shown in Fig. 2 of the main text. Our fitting procedure gives excellent agreement with experiment over the entire temperature range, but it is important to note that it yields considerable parameter codependency, so that the fitted values must be treated with caution (particularly for the pH 7 data). The results presented in Table S4 are our "best-fit" parameters insofar as they yield a minimum χ^2 value over the experimental data points, but a range of parameter combinations would have also produced reasonable fits. The large error bars in some of the parameters are really indicative of significant parameter covariance. This is not an inherent limitation of the fitting procedure: For example, more data would make it possible to better constrain the fits. Nevertheless, the most notable outcome from the fits is the fact that (*i*) they differ considerably from results obtained using an Arrhenius-type fit, and (*ii*) they agree very well with the results obtained from QM/MM calculations.

We note that it would have been possible to fit the data with a more sophisticated multistate (multiconformation) model of the sort required to explain the data in some other enzymes (10, 11); however, in the case of heavy and light DHFR, the multiple-conformer models did not give improved nonlinear least-squares fits compared with single-conformer models. This finding, alongside the good agreement with both experiment and QM/MM simulations based on a single-protein conformation, argues against the involvement of multiple significantly different conformations in the hydride transfer catalyzed by DHFR. Although the fits do not allow us to rule out the presence of multiple conformers conclusively, we are able to state with confidence that the experimental data here can be fitted just as well with a single-conformer model as with a multiconformer model.

QM/MM Ensemble-Averaged Variational Transition-State Theory Calculations and Molecular Dynamics Simulations

The Simulation Model. The starting structure for dynamics simulations was obtained from Protein Data Bank entry 3QL3 for the ternary complex EcDHFR·NADP$^+$·folate (15). The PROPKA3 program (16–19) was used to estimate the pK_a values of the titratable protein residues to verify their protonation states at pH 7; histidines 45, 114, and 141 were doubly protonated whereas all other histidine residues were protonated only on Nδ or Nε. To neutralize the system, 13 sodium counterions were placed in optimal electrostatic positions around the enzyme. Finally, the system was solvated using a cubic box of TIP3P (transferable intermolecular potential 3 point) water molecules with side lengths of 65.2 Å; water molecules with an oxygen atom within 2.8 Å of any heavy atom were removed. The full system contained 27,219 atoms, containing the protein (159 residues, 2,544 atoms), the substrate and cofactor (52 and 74 atoms, respectively), 13 sodium ions, and 8,196 water molecules (24,132 atoms). Heavy EcDHFR was prepared by modifying the masses of all ^{14}N, ^{12}C, and nonexchangeable ^{1}H atoms to those of ^{15}N, ^{13}C, and ^{2}H. The ratio between the masses of the simulated heavy and light enzymes was 1.10987, similar to the experimentally observed molecular weight increase.

The whole system was divided into a QM part and an MM part to perform combined QM/MM calculations (Fig. S3). The quantum subsystem contained 76 atoms, including parts of the cofactor (nicotinamide ring and the ribose) and substrate (pteridine ring and the *N*-methylene-substituted *p*-aminobenzoyl, pABA). Two hydrogen "link" atoms (20) were used to saturate the valence at the QM-MM boundary (Fig. S3). The quantum atoms were treated by the AM1 (Austin Method 1) Hamiltonian (21), modified using specific reaction parameters (denoted as AM1-SRP) developed previously for DHFR (22). The protein atoms and the ions were described by the OPLS-AA (Optimized Potentials for Liquid Simulations - All Atoms) (23) force field whereas the water molecules were described by the TIP3P potential (24). Cutoffs for the nonbonding interactions were applied using a switching function within a radius range of 13.0–9.0 Å. Periodic boundary conditions were used within the minimum image convention in all of the simulations.

PMF. One-dimensional PMFs, W^{CM}, were computed using the antisymmetric combination of distances describing the hydride transfer, $z = d_{C4Ht}–d_{HtC6}$, as the reaction coordinate. The umbrella sampling approach (25) was used, with the system restrained to remain close to the desired value of the reaction coordinate by means of the addition of a harmonic potential with a force constant of 2,500 kJ·mol^{-1}·A^{-2}, which allows good overlap between windows. The reaction coordinate was then explored in a range from –2.07 Å to 1.57 Å, with a window width of 0.07 Å (the total number of windows was 53). The probability distributions obtained from MD simulations within each individual window were combined by means of the weighted histogram analysis method (WHAM) (26). Twenty picoseconds of relaxation and 40 ps of production MD, with a time step of 0.5 fs, in the canonical ensemble [NVT (number, volume, temperature), with a reference temperature of 300 K] and the Langevin–Verlet integrator (27), were used in the simulations.

Five additional PMFs were computed at the AM1-SRP/MM level to check the robustness of our method. The starting structures were selected from snapshots of a long QM/MM MD simulation with the reaction coordinate restrained to the value obtained for the transition state (TS) of the first PMF. The results (Fig. S4*A*) show very small deviations between the profiles and between the averaged structures of the three states involved in the reaction (i.e., all of the reactant structures are similar, all of the TSs are similar to one another, and all of the product states are similar to one another). From these PMFs, the classical mechanical activation free-energy barrier, $W^{\ddagger}$, is 15.8 ± 0.4 kcal·mol^{-1}. In addition to being in good agreement with the fits to the experimental data, the values of $W^{\ddagger}$ are similar to previous PMF calculations (see, for example, refs. 22, 28, 29) It is important to note that the ensemble-averaged variational transition-state theory (EA-VTST) QM/MM calculations were performed for the fully protonated substrate. Therefore, it is appropriate to compare the EA-VTST rate constants with experimental results obtained at pH lower than 6 (*Discussion* in the main text). These values of the rate constants are expected to be approximately fivefold larger than those measured at pH 7 but the corresponding differences in terms of free energies would be smaller than 1 kcal·mol^{-1} (30).

Selected geometries of the reactant state (RS) and the TS were used as starting points to run 2-ns AM1-SRP/MM MD simulations with the reaction coordinate restrained to the corre-

sponding values, to investigate the structural properties of the RS and the TS in more detail. The average values of key geometrical parameters are listed in Table S5. The TS is at a value of the reaction coordinate close to zero (–0.17 Å), with the transferred hydrogen atom slightly closer to the donor carbon atom than to the acceptor one. As expected, the TS is characterized by a shorter distance between the donor and acceptor atoms (2.63 Å) than in the RS (3.93 Å), as well as a more linear arrangement of the three atoms directly involved in the transfer (C_{donor}-H-$C_{acceptor}$ equal to 163° and 141° in the TS and RS, respectively). It is noticeable that some H-bonding groups (Asp27, Ala7, and, in particular, Met20) significantly approach the reacting system as the reaction progresses: Comparing simulations of the RS and the TS, two new H-bonds are established between the sulfur atom of Met20 and N7N and N5 of nicotinamide ring and pteridine ring, respectively, at the TS. The effect of stronger interactions with the amide group of a nicotinamide ring cofactor at the TS than at the RS, already observed in simulations in our laboratory in the study of the hydride transfer between the formate anion and NAD^+ catalyzed by formate dehydrogenase (31), suggests a more stabilizing pattern of interactions in the TS than in the Michaelis complex.

Reactive Trajectory (Activated Dynamics) Simulations. We ran a 2-ns NVT QM/MM MD trajectory restrained to the TS region with a time step of 0.5 fs for the reaction in both enzymes. The simulation temperature was 300 K and one configuration was saved every 10 ps, resulting in 200 configurations that were used to compute free (unrestrained) downhill trajectories. The velocity associated with the reaction coordinate is not properly thermalized in these initial configurations (because of the reaction coordinate restraint). Thus, following a procedure similar to that used by Gao and coworkers (32) and used in our previous studies (31, 33–35), we selectively removed the projection of the velocity on the reaction coordinate and added a random value taken from a Maxwell–Boltzmann distribution.

For each of the saved TS configurations with modified velocities, we ran free molecular dynamics simulations (i.e., with no reaction coordinate restraint) within the microcanonical ensemble (NVE). Separately, for each configuration we integrated the equations of motion forward and backward, just changing the sign of the velocity components. Downhill trajectories were propagated from –2 ps to +2 ps, using a time step of 0.5 fs. The trajectories obtained were then classified as reactive trajectories when reactants connect to products (RP trajectories) or nonreactive trajectories leading either from reactants to reactants (RR) or from products to products (PP). Both reactive and nonreactive trajectories may exhibit recrossings of the dividing surface. To compute the recrossing transmission coefficient, we used the "positive flux" formulation (36), assuming that the trajectory is initiated at the barrier top with forward momentum along the reaction coordinate,

$$\gamma(t) = \frac{\langle j_+ \theta[z(+t)] \rangle - \langle j_+ \theta[z(-t)] \rangle}{\langle j_+ \rangle}, \qquad \textbf{[S2]}$$

where z is the reaction coordinate, j_+ represents the initially positive flux at $t = 0$, given by $z(t = 0)$, and $\theta(z)$ is a step function equal to one in the product side of the reaction coordinate and zero on the reactant side. The average is calculated over all of the trajectories.

Ensemble-Averaged Variational Transition-State Theory. Deviations from classical TST as a result of quantum tunneling effects can be estimated by means of EA-VTST (37–39). In this approach, the theoretical estimation of the rate constant can be written as

$$k_{theor}(T) = \Gamma(T) \frac{k_B T}{h} \exp\left(-\frac{\Delta G^{QC}_{act}}{RT}\right). \qquad \textbf{[S3]}$$

ΔG^{QC}_{act} is the quasiclassical activation free energy at the transition state, obtained from the classical mechanical (CM) PMF and including a correction for quantizing the vibrations orthogonal to the reaction coordinate and the vibrational free energy of the reactant mode that correlates with motion along the reaction coordinate, and is calculated as

$$\Delta G^{QC}_{act} = \left[W^{CM}(T, z^*) + \Delta W_{vib}(T, z^*)\right] - \left[W^{CM}(T, z_R) + \Delta W_{vib,R}(T) + G^{CM}_{R,T,F}\right], \qquad \textbf{[S4]}$$

where $\Delta W_{vib}(T, z^*)$ corrects $W^{CM}(T, z^*)$ to account for quantized vibrations orthogonal to z, the reaction coordinate along which the PMF is defined, at the maximum of the PMF, z^*; $\Delta W_{vib,R}(T)$ corrects $W^{CM}(T, z_R)$ for quantized vibrations at the reactant side minimum of the PMF, z_R, and $G^{CM}{}_{R,T,F}$ is a correction for the vibrational free energy of the reactant mode that correlates with motion along the reaction coordinate (37).

To correct the classical mechanical PMF, W^{CM}, normal mode analyses were performed for the quantum region atoms. ΔG^{QC}_{act}, as described elsewhere (37), is obtained by Eq. **S4**, with the terms defined above. Briefly, the zero-point energy for each mode within the primary zone is obtained by evaluating an ensemble average over primary subsystems and making a quasiharmonic approximation. At each ensemble point, we form a Hessian and project out the reaction coordinate. This allows one to obtain the corresponding vibrational frequencies at each point along the reaction path, averaged over an ensemble that includes the effects of anharmonicity. Quantization of the vibrational frequencies is then obtained as a correction to the classical PMF. In the reactants, zero-point energy is included in the reaction coordinate mode; at the TS, tunneling along the reaction coordinate mode is treated using the small curvature tunneling approximation. To perform these calculations, we localized 13 TS structures, starting from different configurations of the corresponding simulation windows in the heavy and light enzymes. After intrinsic reaction coordinate (IRC) calculations, we optimized the corresponding reactant structures and obtained the Hessian matrix for all of the stationary structures. The final quantum mechanical corrections were obtained as an average over these structures. $W^{‡}$, the PMF difference between the TS and the reactants [$W^{‡} = W^{CM}(T, z^*) - W^{CM}(T, z_R)$], was found to be 15.8 ± 0.4 kcal·mol^{-1}; $G^{CM}{}_{R,T,F}$, the vibrational free energy corresponding to the reaction coordinate at the reactants, was found to be 0.38 ± 0.02 kcal·mol^{-1}; and ΔW_{vib} (T), the correction for quantized vibrations [ΔW_{vib} $(T) = \Delta W_{vib}$ $(T, z^*) - \Delta W_{vib,R}$ (T)], was found to be −1.59 ± 0.10 kcal·mol^{-1}. Further corrections can be found in Table 1 of the main text. The quasiclassical free-energy barrier (i.e., the free energy corrected using zero point energy contributions) and the tunneling contributions, κ, are statistically indistinguishable in the light and heavy enzymes, owing to the fact that the primary zones of the heavy and light enzymes are effectively identical, because only the protein environment (and not the substrate/cofactor) was isotopically substituted in these simulations.

The transmission coefficient, Γ, is obtained as the product of recrossing (γ) and tunneling (κ) contributions:

$$\Gamma(T) = \gamma(T) \cdot \kappa(T). \qquad \textbf{[S5]}$$

The recrossing transmission coefficient, γ, was calculated by randomizing the reaction coordinate velocity for 200 TS configurations, running free downhill MD trajectories and using the positive flux formulation to calculate flux–flux correlation functions (Eq. **S2**).

The tunneling transmission coefficient, κ, was calculated with the small-curvature tunneling (SCT) approximation, which includes reaction-path curvature appropriate for enzymatic hydride transfers (40, 41). Previously, the SCT approximation has been applied successfully to enzymatic reactions, catalyzed by DHFR and aromatic amine dehydrogenase, and produced KIEs and phenomenological activation energies that are in good agreement with the experimental results (40, 41). The final tunneling contribution is obtained as the average over the reaction paths of 13 TS structures.

To test whether the position of the variational transition state is sensitive to the isotope substitution in the light and heavy systems, we expanded the original primary zone beyond the QM atoms of the substrate and cofactor, to include additional nearby residues (ALA7, MET20, ASP27, TYR100, ILE14, and ALA19). The internal reaction coordinate was then followed by stepping along the mass-weighted minimum energy path and reoptimizing both the primary and the secondary regions at each point. Geometry optimizations used a full Hessian in the primary region and gradients within the secondary region. We then added in the effects of mode quantization along the IRC as discussed above. The positions of the free-energy maxima (and thus the variational TS) are essentially identical for the light and heavy enzymes (Fig. S4*B*).

Finally, Eq. **S3** can be transformed into Eq. **S6** by incorporating the transmission coefficient into the exponential term, giving a phenomenological free energy of activation, ΔG_{eff}:

$$k_{\mathrm{theor}}(T) = \frac{k_{\mathrm{B}}T}{h}\exp\left(-\frac{\Delta G_{\mathrm{eff}}}{RT}\right). \qquad \textbf{[S6]}$$

Eq. **S6** folds in effects due to the transmission coefficient as corrections to the effective classical free-energy barrier.

In both the light and the heavy enzymes, the EA-VTST simulations give transmission coefficients reasonably close to unity, indicating that the simple reaction coordinate used here provides an accurate quantitative description of the chemical reaction; if other coordinates were significantly involved, the transmission coefficient would to be considerably smaller than unity (40).

It is important to note that the activated trajectories procedure described above for calculating γ varies slightly from the original EA-VTST prescription (39). That work outlines two different contributions to γ. First is the "stage 2 step 1" transmission coefficient, which is calculated using an ensemble of individual minimum energy paths (MEPs) within a frozen secondary zone. The extent to which individual MEPs vary from the PMF corresponds to how strongly the distinguished reaction coordinate is coupled to other modes within the primary zone. The second contributor to γ in the original EA-VTST framework is the so-called "stage 3" correction, which accounts for the free-energy change of the secondary zone as the system leaves the primary zone variational TS.

The principal difference between the two-stage transmission coefficient procedure outlined in the original EA-VTST procedure and the activated trajectories approach is that the latter allows a straightforward and simultaneous treatment of relaxation within both the primary and the secondary regions. For the system under investigation in this work, we judged this to be a particularly important aspect of the system, because the bulk of the isotopic substitution is within the secondary zone (i.e., the substrate/cofactor upon which the heavy and light proteins act is not isotopically substituted, making the primary zones of the heavy and light enzymes largely identical). Nevertheless, both approaches accomplish a similar goal, and the extent to which the recrossing coefficient deviates from unity provides a metric for how strongly coupled other degrees of freedom are to the distinguished reaction coordinate.

The question of whether the activated trajectories approach can help us to improve the definition of the reaction coordinate is certainly an interesting one. In principle, it should be possible to use our approach to improve the reaction coordinate definition (see, e.g., refs. 33 and 35). Diagonalization of primary zone Hessians might allow resolution of the features in the friction spectrum (Fig. S4*D*). However, for this system, we anticipate that such attempts will be fraught with substantial difficulties for two reasons: (*i*) The friction spectrum (Fig. S4*D*) shows that the most significant differences in heavy/light motions coupled to the hydride transfer reaction coordinate occur below 550 cm^{-1}; and (*ii*) Fig. S4 *E*–*G* shows that the difference in relaxation between the heavy and the light protein environment is difficult to see from inspecting individual dynamical motions; rather, the difference in protein response time can be seen only when one considers a large collection of atomic positions (e.g., in Fig. S4*H*). Both of these facts point to the reaction coordinate being coupled to collective low-frequency protein motions, and it is unlikely that diagonalization of a Hessian for sequentially larger subsets of the atoms surrounding the active space would allow assignment of these motions. Such analyses are usually accurate only for higher-frequency motions.

Calculation of the Friction Spectra. The dynamical coupling of protein motions to the reaction coordinate z can be analyzed in terms of a time-dependent friction $\zeta(t)$ that opposes to the advance of the system along the reaction coordinate. The friction kernel, $\zeta(t)$, can be obtained from the autocorrelation of the forces projected on the reaction coordinate (F_z) obtained from simulations where the system is kept at $z = z^*$ (42),

$$\zeta(t) = \frac{\langle F_z(0)F_z(t)\rangle_{z=z^*}}{\mu_z k_{\mathrm{B}}T}, \qquad \textbf{[S7]}$$

where k_{B} is the Boltzmann constant, T is the temperature, and μ_z is the reduced mass associated with the reaction coordinate. The friction spectrum is then obtained as the Fourier transform of the friction kernel and informs us about the frequency distribution of those motions coupled to the reaction coordinate.

1. Blakley RL (1960) Crystalline dihydropteroylglutamic acid. *Nature* 188:231–232.
2. Swanwick RS, Maglia G, Tey LH, Allemann RK (2006) Coupling of protein motions and hydrogen transfer during catalysis by Escherichia coli dihydrofolate reductase. *Biochem J* 394(Pt 1):259–265.
3. Falzone CJ, et al. (1994) 1H, 15N and 13C resonance assignments, secondary structure, and the conformation of substrate in the binary folate complex of Escherichia coli dihydrofolate reductase. *J Biomol NMR* 4(3):349–366.
4. Swanwick RS, Shrimpton PJ, Allemann RK (2004) Pivotal role of Gly 121 in dihydrofolate reductase from *Escherichia coli*: The altered structure of a mutant enzyme may form the basis of its diminished catalytic performance. *Biochemistry* 43(14):4119–4127.
5. Hay S, et al. (2009) Are the catalytic properties of enzymes from piezophilic organisms pressure adapted? *ChemBioChem* 10(14):2348–2353.
6. Evans RM, et al. (2010) Catalysis by dihydrofolate reductase from the psychropiezophile *Moritella profunda*. *ChemBioChem* 11(14):2010–2017.
7. Stone SR, Morrison JF (1982) Kinetic mechanism of the reaction catalyzed by dihydrofolate reductase from *Escherichia coli*. *Biochemistry* 21(16):3757–3765.
8. Maglia G, Allemann RK (2003) Evidence for environmentally coupled hydrogen tunneling during dihydrofolate reductase catalysis. *J Am Chem Soc* 125(44):13372–13373.
9. Skodje RT, Truhlar DG (1981) Parabolic tunneling calculations. *J Phys Chem* 85:624–628.
10. Glowacki DR, Harvey JN, Mulholland AJ (2012) Protein dynamics and enzyme catalysis: The ghost in the machine? *Biochem Soc Trans* 40(3):515–521.
11. Glowacki DR, Harvey JN, Mulholland AJ (2012) Taking Ockham's razor to enzyme dynamics and catalysis. *Nat Chem* 4(3):169–176.
12. Tresadern G, et al. (2002) Calculations of hydrogen tunneling and enzyme catalysis: A comparison of liver alcohol dehydrogenase, methylamine dehydrogenase and soybean lipoxygenase. *Chem Phys Lett* 358:489–494.
13. Temelso B, Sherrill CD, Merkle RC, Freitas RA, Jr. (2006) High-level ab initio studies of hydrogen abstraction from prototype hydrocarbon systems. *J Phys Chem A* 110(38): 11160–11173.
14. Alhambra C, Corchado JC, Sanchez ML, Gao JL, Truhlar DG (2000) Quantum dynamics of hydride transfer in enzyme catalysis. *J Am Chem Soc* 122:8197–8203.

15. Bhabha G, et al. (2011) A dynamic knockout reveals that conformational fluctuations influence the chemical step of enzyme catalysis. *Science* 332(6026):234–238.
16. Li H, Robertson AD, Jensen JH (2005) Very fast empirical prediction and rationalization of protein pKa values. *Proteins* 61(4):704–721.
17. Bas DC, Rogers DM, Jensen JH (2008) Very fast prediction and rationalization of pKa values for protein-ligand complexes. *Proteins* 73(3):765–783.
18. Sondergaard CR, Olsson MHM, Rostkowski M, Jensen JH (2011) Improved treatment of ligands and coupling effects in empirical calculation and rationalization of pK(a) values. *J Chem Theory Comput* 7:2284–2295.
19. Olsson MHM, Sondergaard CR, Rostkowski M, Jensen JH (2011) PROPKA3: Consistent treatment of internal and surface residues in empirical pK(a) predictions. *J Chem Theory Comput* 7:525–537.
20. Reuter N, Dejaegere A, Maigret B, Karplus M (2000) Frontier bonds in QM/MM methods: A comparison of different approaches. *J Phys Chem A* 104:1720–1735.
21. Dewar MJS, Zoebisch EG, Healy EF, Stewart JJP (1985) The development and use of quantum-mechanical molecular models. 76. AM1 - a new general-purpose quantum-mechanical molecular model. *J Am Chem Soc* 107:3902–3909.
22. Doron D, Major DT, Kohen A, Thiel W, Wu X (2011) Hybrid quantum and classical simulations of the dihydrofolate reductase catalyzed hydride transfer reaction on an accurate semi-empirical potential energy surface. *J Chem Theory Comput* 7:3420–3437.
23. Kaminski GA, Friesner RA, Tirado-Rives J, Jorgensen WL (2001) Evaluation and reparametrization of the OPLS-AA force field for proteins via comparison with accurate quantum chemical calculations on peptides. *J Phys Chem B* 105: 6474–6487.
24. Jorgensen WL, Chandrasekhar J, Madura JD, Impey RW, Klein ML (1983) Comparison of simple potential functions for simulating liquid water. *J Chem Phys* 79:926–935.
25. Torrie GM, Valleau JP (1977) Non-physical sampling distributions in Monte-Carlo free-energy estimation - umbrella sampling. *J Comput Phys* 23:187–199.
26. Kumar S, Bouzida D, Swendsen RH, Kollman PA, Rosenberg JM (1992) The weighted histogram analysis method for free-energy calculations on biomolecules. 1. The method. *J Comput Chem* 13:1011–1021.
27. Verlet L (1967) Computer experiments on classical fluids. 1. Thermodynamical properties of Lennard-Jones molecules. *Phys Rev* 159(1):98–103.
28. Garcia-Viloca M, Truhlar DG, Gao J (2003) Reaction-path energetics and kinetics of the hydride transfer reaction catalyzed by dihydrofolate reductase. *Biochemistry* 42(46):13558–13575.
29. Boekelheide N, Salomón-Ferrer R, Miller TF, 3rd (2011) Dynamics and dissipation in enzyme catalysis. *Proc Natl Acad Sci USA* 108(39):16159–16163.
30. Fierke CA, Johnson KA, Benkovic SJ (1987) Construction and evaluation of the kinetic scheme associated with dihydrofolate reductase from *Escherichia coli*. *Biochemistry* 26(13):4085–4092.
31. Roca M, Oliva M, Castillo R, Moliner V, Tuñón I (2010) Do dynamic effects play a significant role in enzymatic catalysis? A theoretical analysis of formate dehydrogenase. *Chemistry* 16(37):11399–11411.
32. Nam K, Prat-Resina X, Garcia-Viloca M, Devi-Kesavan LS, Gao JL (2004) Dynamics of an enzymatic substitution reaction in haloalkane dehalogenase. *J Am Chem Soc* 126(5): 1369–1376.
33. Roca M, Moliner V, Tuñón I, Hynes JT (2006) Coupling between protein and reaction dynamics in enzymatic processes: Application of Grote-Hynes Theory to catechol O-methyltransferase. *J Am Chem Soc* 128(18):6186–6193.
34. Castillo R, Roca M, Soriano A, Moliner V, Tuñón I (2008) Using Grote-Hynes theory to quantify dynamical effects on the reaction rate of enzymatic processes. The case of methyltransferases. *J Phys Chem B* 112(2):529–534.
35. Ruiz-Pernía JJ, Tuñón I, Moliner V, Hynes JT, Roca M (2008) Dynamic effects on reaction rates in a Michael addition catalyzed by chalcone isomerase. Beyond the frozen environment approach. *J Am Chem Soc* 130(23):7477–7488.
36. Bergsma JP, Gertner BJ, Wilson KR, Hynes JT (1987) Molecular dynamics of a model SN2 reaction in water. *J Chem Phys* 86:1356–1376.
37. Alhambra C, et al. (2001) Canonical variational theory for enzyme kinetics with the protein mean force and multidimensional quantum mechanical tunneling dynamics. Theory and application to liver alcohol dehydrogenase. *J Phys Chem B* 105:11326–11340.
38. Truhlar DG, et al. (2002) The incorporation of quantum effects in enzyme kinetics modeling. *Acc Chem Res* 35(6):341–349.
39. Truhlar DG, et al. (2004) Ensemble-averaged variational transition state theory with optimized multidimensional tunneling for enzyme kinetics and other condensed-phase reactions. *Int J Quantum Chem* 100:1136–1152.
40. Pu J, Gao J, Truhlar DG (2006) Multidimensional tunneling, recrossing, and the transmission coefficient for enzymatic reactions. *Chem Rev* 106(8):3140–3169.
41. Pang JY, Pu JZ, Gao JL, Truhlar DG, Allemann RK (2006) Hydride transfer reaction catalyzed by hyperthermophilic dihydrofolate reductase is dominated by quantum mechanical tunneling and is promoted by both inter- and intramonomeric correlated motions. *J Am Chem Soc* 128(24):8015–8023.
42. Gertner BJ, Wilson KR, Hynes JT (1989) Nonequilibrium solvation effects on reaction rates for model SN2 reactions in water. *J Chem Phys* 90:3537–3558.

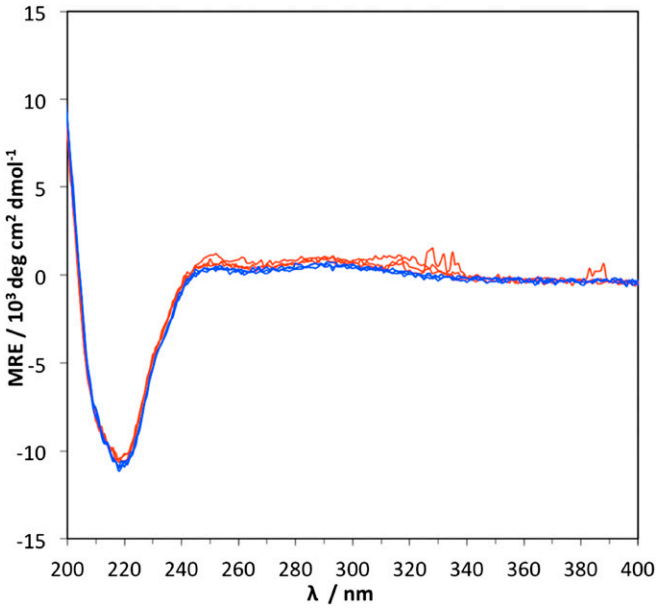

Fig. S1. Circular dichroism spectroscopy of light (red) and heavy (blue) EcDHFR (three scans each), measured in 10 mM potassium phosphate at pH 7, using 14 μM protein.

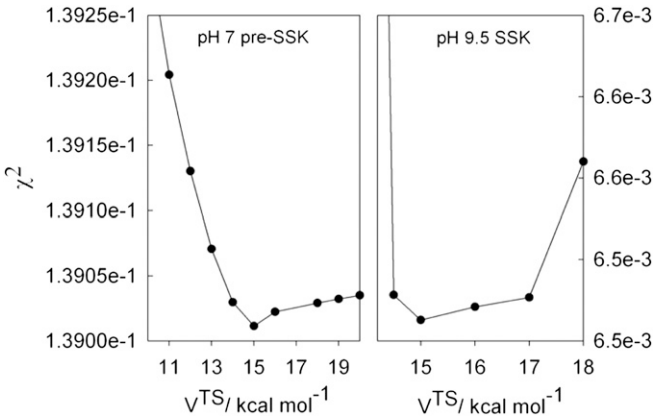

Fig. S2. χ^2 values obtained by fitting the hydride transfer kinetics data to Eq. **3** and Eq. **S1**. The plots were constructed by scanning along V^{TS} and floating all other parameters in Eq. **3** and Eq. **S1**. *Left* and *Right* show χ^2 obtained from fits to the pH 7.0 pre–steady-state kinetic data and the pH 9.5 steady-state kinetic data, respectively. At each pH, the fit shows a χ^2 minimum around $V^{TS} = 15$ kcal·mol^{-1}.

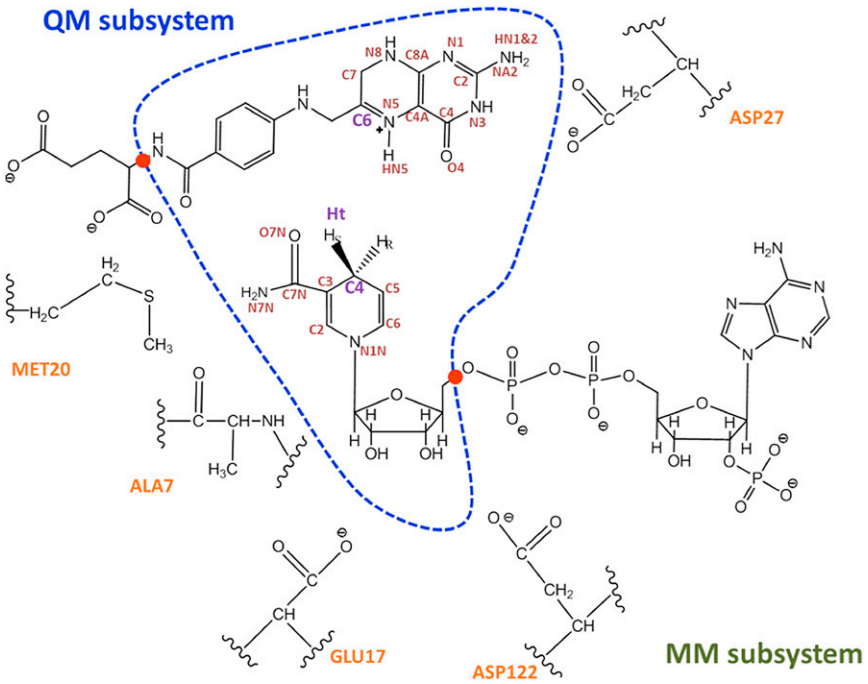

Fig. S3. QM/MM partitioning scheme. Red circles represent the quantum hydrogen link atoms. Atoms in the nicotinamide ring and the pteridine ring, most notably the transferred hydride, Ht, and its donor and acceptor carbon atoms, have been labeled.

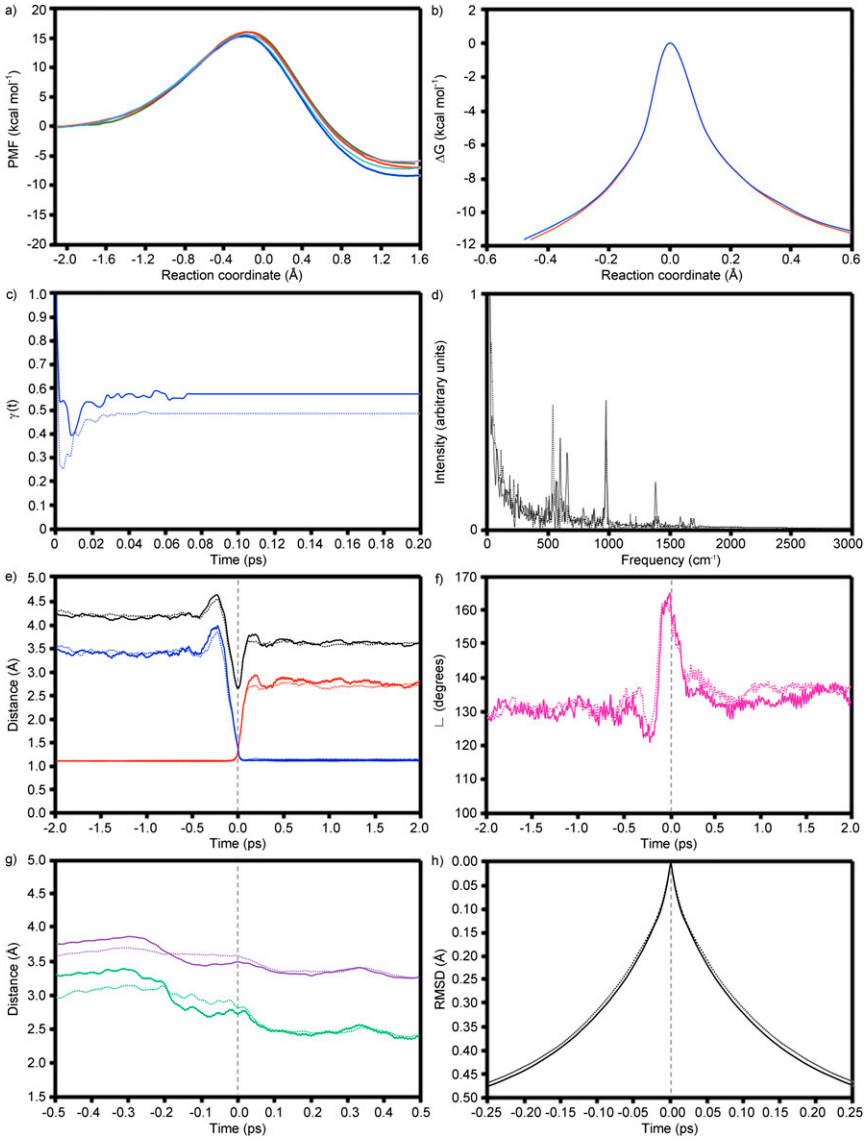

Fig. S4. (*A*) Classical mechanical AM1-SRP/MM potential of mean force (PMF) obtained from five different structures of the TS (different colors are used to indicate PMFs calculated from different starting structures). The starting structures were selected (and subsequently optimized) from a restrained MD simulation of the initial TS structure (main text). This plot shows that the PMFs are well converged. (*B*) Free-energy profiles obtained for the light (red line) and heavy (blue line) enzymes, including the free-energy contribution of the vibrations of the reacting system and surrounding residues to the IRC. The values of the free energy and the reaction coordinate are relative to the light enzyme maxima. This plot shows that the position of the transition state is not affected by variational optimization of the TS; after several trials we found that the change in the position of the variational optimized transition state between the light and heavy enzyme is definitely below 0.01 Å. (*C–H*) Important features of the reaction in the vicinity of the transition state, from simulations of hydride transfer in light (solid lines) and heavy EcDHFR (dashed lines). (*C*) time-dependent evolution of the recrossing transmission coefficients, $\gamma(t)$; (*D*) friction spectra, showing the frequency distribution of motions that are coupled to the reaction coordinate (*SI Text*); (*E*) distances between the C4-C6 (black line), C4-Ht (red line), and C6-Ht (blue line) atoms involved in the chemical reaction; (*F*) angle C4-Ht-C6; (*G*) distances between S_{Met20} and H of $N7N_{NADPH}$ (green line) and between S_{Met20} and $N7N_{NADPH}$ (mauve line); (*H*) averaged evolution of the RMSD (calculated by considering all atoms) from the TS structure in reactive trajectories. For *E–H*, the system is at the top of the barrier at $t = 0$, whereas increasingly negative and positive times correspond to evolution toward the reactant and product states, respectively.

Table S1. Temperature dependence of the steady-state rate constants and enzyme KIEs at pH 9.5 and pH 7 (k_{cat}) and the pre–steady-state rate constants and enzyme KIEs at pH 7 (k_H) for reaction in light and heavy EcDHFR

	Steady state, pH 9.5			Presteady state, pH 7.0			Steady state, pH 7.0		
T (°C)	k_{cat}^{LE}, s^{-1}	k_{cat}^{HE}, s^{-1}	$k_{cat}^{LE}/k_{cat}^{HE}$	k_H^{LE}, s^{-1}	k_H^{HE}, s^{-1}	k_H^{LE}/k_H^{HE}	k_{cat}^{LE}, s^{-1}	k_{cat}^{HE}, s^{-1}	$k_{cat}^{LE}/k_{cat}^{HE}$
7	0.33 ± 0.03	0.32 ± 0.03	1.03 ± 0.07	77.4 ± 1.5	83.7 ± 3.2	0.92 ± 0.04			
10	0.49 ± 0.02	0.43 ± 0.03	1.13 ± 0.04	89.3 ± 1.1	95.9 ± 2.6	0.93 ± 0.01	1.28 ± 0.17	1.31 ± 0.10	0.98 ± 0.09
15	0.80 ± 0.07	0.72 ± 0.07	1.10 ± 0.07	103.1 ± 4.3	113.5 ± 1.7	0.91 ± 0.03	2.12 ± 0.15	2.11 ± 0.17	1.01 ± 0.04
20	1.13 ± 0.15	1.06 ± 0.17	1.06 ± 0.06	119.1 ± 2.7	130.0 ± 1.2	0.92 ± 0.04	3.73 ± 0.11	3.60 ± 0.10	1.04 ± 0.03
25	1.86 ± 0.18	1.64 ± 0.16	1.13 ± 0.08	178.2 ± 4.7	151.6 ± 4.2	1.10 ± 0.03	6.86 ± 0.10	6.49 ± 0.49	1.06 ± 0.01
30	2.76 ± 0.25	2.42 ± 0.24	1.14 ± 0.08	209.1 ± 5.0	190.1 ± 8.5	1.10 ± 0.04	15.53 ± 0.55	13.95 ± 0.38	1.11 ± 0.03
35	3.71 ± 0.23	3.13 ± 0.24	1.18 ± 0.06	248.3 ± 5.3	232.5 ± 3.9	1.07 ± 0.07	23.81 ± 0.31	20.50 ± 0.50	1.16 ± 0.01
40	5.40 ± 0.15	4.25 ± 0.22	1.27 ± 0.04	329.5 ± 19.5	279.5 ± 15.0	1.18 ± 0.09	37.18 ± 0.83	32.33 ± 0.18	1.15 ± 0.02

Table S2. Steady-state kinetic parameters for light and heavy EcDHFR at 20 °C and 35 °C

	pH 9.5		pH 7	
Parameter	Light	Heavy	Light	Heavy
At 20 °C				
k_{cat}, s^{-1}	1.13 ± 0.15	1.06 ± 0.17	3.73 ± 0.11	3.60 ± 0.10
K_M NADPH, μM	1.86 ± 0.20	1.89 ± 0.30	5.10 ± 0.74	4.04 ± 0.39
K_M DHF, μM	1.15 ± 0.27	1.29 ± 0.34	1.05 ± 0.12	0.53 ± 0.08
At 35 °C				
k_{cat}, s^{-1}	3.71 ± 0.23	3.13 ± 0.24	23.8 ± 0.3	20.5 ± 0.5
K_M NADPH, μM	6.54 ± 1.47	5.74 ± 0.74	11.5 ± 2.6	11.3 ± 2.2
K_M DHF, μM	3.73 ± 0.88	2.78 ± 0.86	1.47 ± 0.12	1.56 ± 0.37

Table S3. pH dependence of the pre–steady-state rate constant (k_H) for reaction in light and heavy EcDHFR at 20 °C and 35 °C

	20 °C		35 °C	
pH	k_H^{LE}, s^{-1}	k_H^{HE}, s^{-1}	k_H^{LE}, s^{-1}	k_H^{HE}, s^{-1}
9	0.72 ± 0.02	0.75 ± 0.08	5.9 ± 0.3	3.4 ± 0.3
8.5	22.0 ± 1.3	23.5 ± 3.8	38.7 ± 1.1	32.0 ± 0.9
8	30.2 ± 0.9	33.3 ± 2.2	107.5 ± 1.1	104.9 ± 1.5
7.5	64.0 ± 1.0	57.9 ± 1.2	163.8 ± 2.1	158.5 ± 1.1
7	152.5 ± 1.5	156.7 ± 2.5	248.3 ± 5.3	232.5 ± 3.9
6.5	207.7 ± 5.7	216.3 ± 3.1	425.4 ± 7.0	416.5 ± 3.7
6	306.0 ± 6.8	317.2 ± 3.1	530.5 ± 17.2	535.5 ± 14.5
5.5	365.0 ± 9.5	377.0 ± 3.5	1,157.0 ± 25.0	1,149.0 ± 57.8
5	447.1 ± 26.5	437.3 ± 4.5	1,400.3 ± 70.0	1,274.0 ± 120.0

Table S4. Best set of parameters giving the fits shown in Fig. 2 of the main text, using Eq. 3 and Eq. S1

	Using Eq. **3** and Eq. **S1***		Arrhenius-like fits†	
Parameters	pH 7	pH 9.5	pH 7	pH 9.5
C^{LE}, $K^{-1}\cdot s^{-1}$	$1.11^{+51.9}_{-1.10}\times10^{9}$	$1.31^{+2.86}_{-1.30}\times10^{9}$	$2.46^{+1.55}_{-1.55}\times10^{4}$	$5.14^{+2.05}_{-2.05}\times10^{7}$
C^{HE}, $K^{-1}\cdot s^{-1}$	$1.03^{+47.5}_{-1.02}\times10^{9}$	$1.15^{+2.31}_{-1.14}\times10^{9}$	$2.46^{+1.55}_{-1.55}\times10^{4}$	$4.55^{+1.07}_{-1.07}\times10^{7}$
ε^{LE}, kcal·mol^{-1}	$14.6^{+10.1}_{-10.1}$	$16.2^{+1.82}_{-1.82}$	$6.33^{+0.37}_{-0.37}$	$13.57^{+0.24}_{-0.24}$
ε^{HE}, kcal·mol^{-1}	$14.6^{+9.5}_{-9.5}$	$16.2^{+1.82}_{-1.82}$	$6.33^{+0.35}_{-0.35}$	$13.57^{+0.21}_{-0.21}$
V^{TS}, kcal·mol^{-1}	15.0‡	15.0‡	—	—
ω^{LE}, cm^{-1}	1296^{+408}_{-408}	1000^{+204}_{-204}	—	—
ω^{HE}, cm^{-1}	1296^{+388}_{-388}	1000^{+189}_{-189}	—	—

Errors shown are SEs (σ) obtained during the least-squares fitting procedure. The uncertainty in some of the parameters is large, owing to considerable parameter codependency; see *SI Text* for a discussion of errors and parameter covariance.
*In these fits, all of the parameters were floated.
†In these fits, we constrained $\kappa^{HE}(T) = \kappa^{LE}(T) = 1$ in Eq. **3**, giving an Arrhenius-like fit of the form $CT\exp(-\varepsilon/RT)$.
‡Value was fixed at 15.0 to correspond to the χ^2 minima obtained in relaxed scans (Fig. S2).

Table S5. Key averaged structural parameters of the reactant state, RS, and transition state, TS, from 2-ns MD simulations at the AM1-SRP/MM level of the RS and the TS at 300 K

Parameter	RS	TS
Reaction coordinate: (C_{donor}-H)-($C_{acceptor}$-H)	−1.95 ± 0.36	−0.17 ± 0.04
Distance C_{donor}-$C_{acceptor}$	3.93 ± 0.25	2.63 ± 0.06
Distance C_{donor}-H	1.09 ± 0.03	1.25 ± 0.03
Distance $C_{acceptor}$-H	3.05 ± 0.36	1.41 ± 0.04
Angle C_{donor}-H-$C_{acceptor}$	141 ± 15	163 ± 7
Distance $OD2_{ASP27}$-$N3_{substrate}$	2.74 ± 0.12	2.82 ± 0.16
Distance $OD1_{ASP27}$-NA2 $_{substrate}$	2.81 ± 0.14	2.76 ± 0.12
Distance S_{MET20}-$N7N_{cofactor}$	4.30 ± 0.50	3.40 ± 0.30
Distance S_{MET20}-$N5_{substrate}$	3.76 ± 0.35	3.70 ± 0.33
Distance O_{ALA7}-$N7N_{cofactor}$	3.68 ± 0.28	3.11 ± 0.19
Distance O_{ALA7}-S_{MET20}	6.36 ± 0.48	5.93 ± 0.41

Distances are in angstroms and angles in degrees.